ELECTRICAL SIZING OF PARTICLES IN SUSPENSIONS

I. THEORY

N. B. GROVER, J. NAAMAN, S. BEN-SASSON, *and* F. DOLJANSKI

From the Department of Experimental Medicine and Cancer Research, The Hebrew University–Hadassah Medical School, Jerusalem, Israel

ABSTRACT The processes involved during the passage of a suspended particle through a small cylindrical orifice across which exists an electric field are considered in detail. Expressions are derived for the resulting change in current in terms of the ratios of particle to orifice volume and particle to suspending fluid resistivity, and particle shape. Graphs are presented of the electric field and of the fluid velocity as functions of position within the orifice, and of the shape factor of spheroids as a function of their axial ratio and orientation in the electric field. The effects of the electric and hydrodynamic fields on the orientation of nonspherical particles and on the deformation of nonrigid spheres is treated, and the migration of particles towards the orifice axis is discussed. Oscillograms of current pulses produced by rigid, nonconducting spheres in various orifices are shown and compared with the theoretical predictions.

INTRODUCTION

The properties of many materials are strongly influenced by particle size, and the size of a living cell is often a reflection of its physiological state. Thus the development by Coulter (1) of an electric transducer for detecting the size of a particle suspended in an electrolytic medium was of major importance as it provided for the first time a rapid and convenient approach to particle size analysis on large samples.

This transducer consists of a small orifice through which the suspension is pumped, producing a change in electrical resistance as each particle traverses the orifice. Simplified theoretical calculations by Kubitschek (2) predict that the fractional change in resistance be equal to the ratio of particle volume to orifice volume for small, high-resistivity particles of any shape. A more refined treatment by Gregg and Steidley (3) shows these calculations to be in error by 50% for spherical particles and by even more for nonspherical particles. The dimensions of orifices usually used for the transduction are such as to make routine application of resistance–resistivity relationships impossible, and recourse must be had to more basic expressions that take edge effects into account. The present series of papers is an

attempt to evaluate theoretically and experimentally the electrical and hydrodynamic factors involved in the transduction of particle size into resistance change in such orifices. (The contribution of any fixed charge on the particles is expected to be small at normal ionic strengths and will not be dealt with.) This paper, the first in the series, provides the necessary theoretical background; subsequent papers will test the applicability of the theory to several types of particles and living cells.

THE ELECTRIC FIELD

In order to understand the relationship between resistance change and particle size it is first necessary to consider the characteristics of the electric field within an orifice joining two infinite electrolytes between which there exists a potential difference. This problem cannot be solved exactly, but lower and upper bounds to the resistance can be obtained by applying suitable constraints to the potential and potential gradient, respectively (4, 5). In order to obtain an upper bound, we follow the approach developed by Lord Rayleigh in the theory of sound for the kinetic energy at the open end of a tube (6). One begins by assuming that the potential gradient in the axial direction at the mouth of the orifice is of the form

$$\frac{d\phi}{dx} \propto 1 + \alpha \frac{r^2}{R^2} + \beta \frac{r^4}{R^4}, \tag{1}$$

where ϕ is the potential, R is the radius of the (cylindrical) orifice, r is the radial coordinate measured from the axis, x is the axial coordinate measured from the mouth, and α and β are constants to be determined by the requirement that the generation of heat be a minimum. The boundary conditions are that the axial component of the potential gradient be uniform far from the mouth of the orifice ($x \gg R$), and that the radial component vanish at the walls of the orifice ($r = R$).

The solution of Laplace's equation with these boundary conditions is given by

$$\phi \propto -\left(1 + \frac{1}{2}\alpha + \frac{1}{3}\beta\right)\frac{x}{R} - 4\sum \frac{\alpha + 2\beta(1 - 8/\zeta^2)}{\zeta^3 J_0(\zeta)} e^{-\zeta(x/R)} J_0\left(\zeta \frac{r}{R}\right), \tag{2}$$

where ζ is a root of the equation $J_0'(\zeta) = 0$ and the summation is to be carried out over all possible values of ζ. Since the current density is equal to $(1/\rho_2)(-d\phi/dx)$, where ρ_2 is the (homogeneous) resistivity of the electrolyte, and having specified the potential completely (except for a constant of proportionality that depends on the applied potential difference), we are now in a position to calculate the resistance Ω from the heat generated:

$$\Omega = 2\frac{\frac{1}{\rho_2}\int_0^R \phi(-d\phi/dx)2\pi r dr \Big|_{x=0} - \frac{1}{\rho_2}\int_0^R \phi(-d\phi/dx)2\pi r dr \Big|_{x\gg R}}{\left[\frac{1}{\rho_2}\int_0^R (-d\phi/dx)2\pi r dr\right]^2}. \tag{3}$$

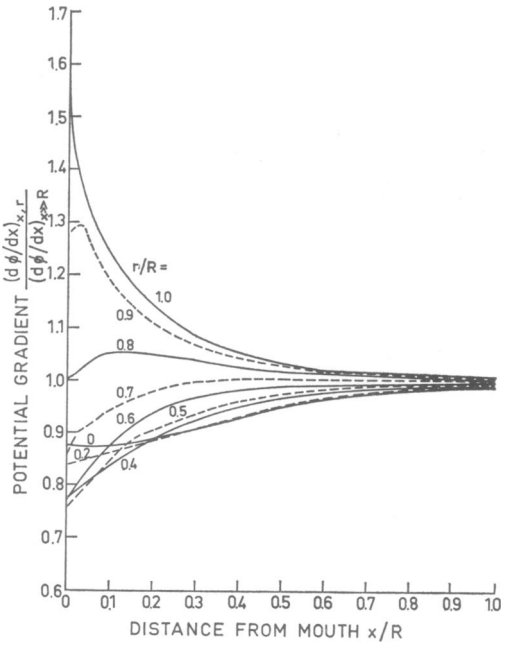

FIGURE 1 Potential gradient $d\phi/dx$ in a cylindrical orifice as a function of distance x from mouth of orifice at various distances r from orifice axis. Potential gradient is expressed relative to its value far from mouth ($x \gg R$); lengths are expressed in units of orifice radius R. Alternate curves are drawn as dashed lines for the purposes of clarity.

By exploiting certain properties of the Bessel functions and their derivatives, one arrives at an expression for Ω that is easily minimized (6) with respect to α and β; the resulting equations in α and β can then be solved explicitly, giving $\alpha = -1.01171$ and $\beta = 1.95125$ as the only set of real roots.

A lower bound to the resistance (4) is obtained by assuming constant potential over the inlet and over the exit of the orifice. This leads to a resistance value that differs from the upper bound value by less than 5%, and Rayleigh (6) suggests that the upper bound is probably within $\frac{1}{2}$% of the true value. Thus the use of equation 2 should not lead to any appreciable error.

Fig. 1 is a plot of $d\phi/dx$ as a function of x/R for various values of r/R. The solution is of course symmetrical about the center of the orifice and is valid only when the orifice is sufficiently long to permit $d\phi/dx$ to attain a value that is independent of x and r. From the figure this is seen to occur at values of x greater than R, so that the length of the orifice must be greater than its diameter.

If we now consider the effect on ρ_2 as a rigid spherical particle of resistivity ρ_1 passes through the region of uniform potential gradient, we can make use of an expression originally derived by Maxwell (7) for the effective resistivity ρ' of a compound medium, namely

$$\rho' = \frac{\rho_1 + \frac{1}{2}\rho_2 + \frac{1}{2}(\rho_1 - \rho_2)\delta}{\rho_1 + \frac{1}{2}\rho_2 - (\rho_1 - \rho_2)\delta}\rho_2, \qquad (4)$$

where δ is the ratio of the volume of the particle to that of the orifice. This equation is strictly true only for $\delta \ll 1$, but by considering terms of higher order than did Maxwell (8–10), one can obtain an expression for ρ' that involves higher powers of δ and is valid for $\delta \lesssim 0.5$. This expression, verified experimentally (10), reduces to equation 4 for all values of ρ_1/ρ_2 provided that $3(a/R')^{10} \ll 1$, where a is the particle radius and R' is the radius of the largest concentric sphere in which $d\phi/dx$ is uniform in the absence of the particle. (The restriction on a/R' becomes less severe as $\rho_1 \rightarrow \rho_2$.)

From the requirement that the particle be in the region of uniform potential gradient it follows that the relative change in current $\Delta I/I$ is equal to $(\rho_2 - \rho')/\rho_2$ and if, in addition, $\rho_1 \gg \rho_2$ then we obtain

$$-\frac{\Delta I}{I} = \frac{\Delta\rho}{\rho_2} \equiv \frac{\rho' - \rho_2}{\rho_2} = \frac{1.5\delta}{1 - \delta} \equiv 1.5\delta'. \tag{5}$$

An extension of Maxwell's solution to include ellipsoidal particles has been obtained by Fricke (11–13) and verified experimentally by Velick and Gorin (14). The case of spheroids (11) is particularly simple and of wide application, and the results will be repeated here. The analog to equation 4 is

$$\rho' = \frac{\rho_1 + (\gamma - 1)\rho_2 + (\gamma - 1)(\rho_1 - \rho_2)\delta}{\rho_1 + (\gamma - 1)\rho_2 - (\rho_1 - \rho_2)\delta}\rho_2 \tag{6}$$

which reduces to

$$\frac{\Delta\rho}{\rho_2} = \gamma\delta' \tag{7}$$

in the case where $\rho_1 \gg \gamma\rho_2$. For an oblate spheroid (principal axes a, b, b and $m \equiv a/b < 1$)

$$\frac{1}{\gamma} = \frac{m \cos^{-1} m}{(1 - m^2)^{3/2}} - \frac{m^2}{1 - m^2} \tag{8}$$

while for a prolate spheroid (principal axes a, b, b and $m \equiv a/b > 1$)

$$\frac{1}{\gamma} = \frac{m^2}{m^2 - 1} - \frac{m \cosh^{-1} m}{(m^2 - 1)^{3/2}}. \tag{9}$$

These equations are, of course, identical and apply when the a-axis is in the x-direction; when either of the b-axes is in the x-direction, then γ must be replaced by γ' in equations 6 and 7, where

$$\gamma' \equiv \frac{2\gamma}{2\gamma - 1}. \tag{10}$$

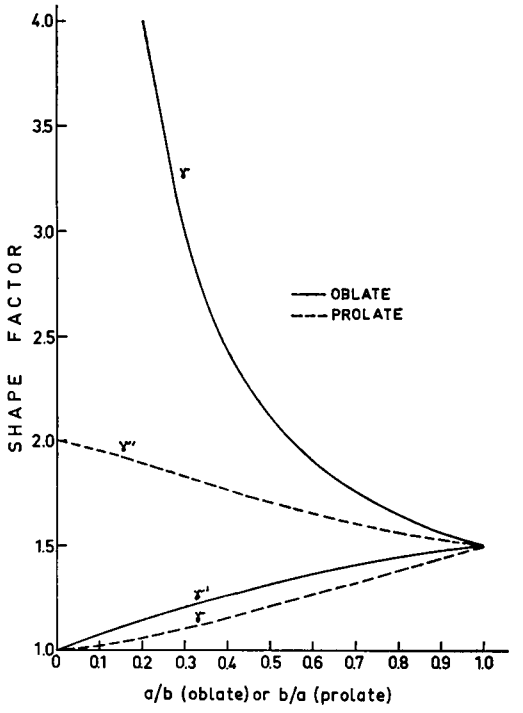

FIGURE 2 Shape factors γ and γ' for an oblate (solid curves) and prolate (dashed curves) spheroid with principal axes a, b, b as a function of axial ratio a/b (oblate) or b/a (prolate). γ: a-axis oriented parallel to orifice axis. γ': either of b-axes parallel to orifice axis.

The value of γ (and hence γ') depends only on the shape of the particle and is completely independent of its volume and of electrolyte resistivity (13). For spherical particles, $\gamma = \gamma' = 1.5$ and equations 6 and 7 reduce to equations 4 and 5, as expected. For nonspherical particles, the factor 1.5 in equation 5 must be replaced by γ or γ', depending on orientation. Fig. 2 shows γ and γ' as functions of a/b for both oblate ($a < b$) and prolate ($a > b$) spheroids.

The contribution of edge effects and electrolyte resistance outside the orifice can readily be taken into account by defining a length l greater than the geometrical length of the orifice and such that the total measured resistance between the electrodes in the absence of the particle is equal to $\rho_2 l/\pi R^2$, and then using $\pi R^2 l$ as the effective orifice volume in the definition of δ. It may be helpful to note that in the absence of a particle the system is electrically equivalent to a perfect cylinder of radius R and length l with equipotentials at each end ($x = 0$, $x = l$) and containing an electrolyte of resistivity ρ_2 ; the effect of a particle of volume v is merely to alter l, changing the volume of the cylinder by an amount equal to $\gamma v/[1 + \gamma\rho_2/(\rho_1 - \rho_2) - \delta]$. This quantity, which may be termed the electrical size of the particle, reduces to $\gamma v/(1 - \delta)$ for $\rho_1 \gg \gamma\ \rho_2$ and is negative for conducting particles ($\rho_1 < \rho_2$).

The orientation of spheroidal particles in an electric field has been treated theoretically by Demetriades (15) and extended by Chaffey and Mason (16). Experimental verification is available for rigid rods (17) and discs (16) in Couette flow.

As will be shown in the following section, the fluid shear is zero throughout most of the orifice. Under such conditions, a uniform potential gradient in the axial direction will change the orientation ψ of the axis of revolution of the spheroid with respect to the axis of the orifice according to the expression (16)

$$\ln \frac{\tan \psi}{\tan \psi_0} = 2P(q, m)K_2 \eta_2^{-1}E^2t \ , \tag{11}$$

where η_2 is the viscosity of the electrolyte, E is the potential gradient in electrostatic units, ψ_0 is the value of ψ at time $t = 0$, K_1 and K_2 are the dielectric constants of the particle and electrolyte, respectively, and $P(q, m)$ is given by

$$P(q, m) = \frac{[2m^2(1 - \gamma) - 1](2\gamma - 3)(q - 1)}{32\pi[q(1 - \gamma) - 1](q + 2\gamma - 1)(m^2 + 1)} \ , \tag{12}$$

with $q \equiv K_1/K_2$. The function P is discussed in reference 16 and for $K_1 \gg K_2$ its absolute value is less than 0.025. Substituting in equation 11 we find that the spheroid begins to rotate from $\psi_0 = \pi/4$ at approximately $1°/\mu$sec for a potential gradient of 2kv/cm, the rotation decreasing as ψ approaches its limiting value (0 for prolate, $\pi/2$ for oblate spheroids) so that to reach to within 5° of this limiting value requires about 70 μsec.

In the event that the particle is not rigid, one must also consider the effect of the potential gradient on particle shape. In order to obtain an indication of the deformation to be expected, let us look at a nonrigid spherical particle of radius a in a uniform potential gradient. This case has been treated theoretically and experimentally by Allan and Mason (18), and they conclude that the sphere will undergo a deformation D given by

$$D \equiv \frac{m - 1}{m + 1} = \frac{9aK_2}{64\pi\tau}\left(\frac{q - 1}{q + 2}\right)^2 E^2, \tag{13}$$

where τ is the interfacial tension. For $q > 1$ the sphere becomes prolate and for $q < 1$ the sphere becomes oblate, its axis of revolution lying parallel to E. In the case of fluid particles the deformation can become appreciable (18), but for suspensions of biological cells the substitution of accepted values for (19) the interfacial tension ($\lesssim 1$ dyne/cm) and (20) the dielectric constants of cells ($q \gg 1$) and (21) aqueous salt solutions (≈ 75) shows that the deformation should be less than 1% for cells below 10 μ in diameter for fields up to 2kv/cm.

It should be noted that both equation 11 and equation 13 involve the potential gradient, and we have seen above that due to the small dimensions of the orifice, this is not uniform but depends on the x, r coordinates. Thus, strictly speaking, the value of E to be used in the above equations is the value of $d\phi/dx$ calculated from equation 2 at the particular values of x/R and r/R being considered and, as can be

seen from Fig. 1, this may alter the value of ln (tan ψ) or D by as much as 50% near the mouth of the orifice.

THE HYDRODYNAMIC FIELD

In order to understand the changes in current produced by a particle as it progresses through the orifice, it is necessary to be able to predict the path it will follow. If the suspension were not pumped through the orifice, the particle would move in the direction of the potential gradient with its electrophoretic mobility, and the probability of its being at any particular value of r could easily be calculated as a function of x. Pumping is necessary, however, in order to remove the electrolyte from within the orifice before it becomes overheated and in order to increase the flow rate of particles and thereby reduce the length of an experiment to reasonable values. As a result, the path followed by the particle does not depend on the electric but on the hydrodynamic field which, in addition, may also contribute markedly to the orientation and deformation effects discussed above. Consequently we now turn to a consideration of the hydrodynamic field created within the orifice by the pumping action.

As a start, let us calculate the tube Reynolds number $\mathfrak{R}$ for the flow within the orifice. For a cylindrical pipe of radius R

$$\mathfrak{R} = Ru_m/\nu \tag{14}$$

where u_m is the mean linear velocity of the fluid and ν its kinematic viscosity. Since u_m is just the volume flow rate per unit cross-sectional area, it is readily determined experimentally; typical values substituted into equation 14 show that $\mathfrak{R}$ is well below 1000 for all values of pressure and orifice size commonly employed. This suggests that the velocity profile be parabolic. But parabolic (Poiseuille) flow requires a certain distance over which to develop, and this distance usually exceeds the actual length of the orifice. It is thus necessary to consider the hydrodynamics in the region preceding complete parabolic flow. As an approximation, one can assume that the axial velocity is uniform across the entrance of the orifice. (When an upper bound to the flow resistance is calculated with this same approximation (4), the result differs from the lower bound by 8% and from the upper bound as calculated by methods used in the previous section by 3%; Rayleigh (6) estimates that it is less than 4% from the true value.) With this approximation, which really applies to short trumpet-shaped entrances where the influence of friction is neglected, the velocity at entry is constant over the cross-section but zero at the walls. The thickness of the layer adjacent to the walls in which the flow is retarded as a result of the finite viscosity of the fluid, the so called boundary layer, increases downstream until (for sufficiently long tubes) it becomes equal to the radius of the orifice; from that distance on, we have complete parabolic flow.

The velocity distribution near the entrance of a circular orifice under the assumption that the flow is laminar, has been obtained by Tatsumi (22) by a process of iteration. His results agree fairly well (23) with previous calculations (24) and with experiments (25–27) and show that under suitable transformations to dimensionless variables, the velocity profile becomes similar throughout the orifice. As this type of calculation is expected to be about as accurate as more elaborate ones (23), we reproduce here the main results pertinent to our problem. The axial velocity $u(x, r)$ is given by the equations

$$\begin{aligned} u/u_1 &= 0.571y/\lambda, & 0 \leq y/\lambda \leq 0.63 \\ u/u_1 &= 1 - (1.025\text{–}0.357y/\lambda)^2, & 0.63 \leq y/\lambda \leq 2.87 \\ u/u_1 &= 1, & 2.87 \leq y/\lambda \end{aligned} \tag{15}$$

where u_1 is the axial velocity in the core region (the region about the axis where u is independent of r), y is a dimensionless variable given by

$$y \equiv \frac{1}{2}\left(1 - \frac{r^2}{R^2}\right), \tag{16}$$

and λ is the displacement thickness of the boundary layer as defined by

$$\lambda \equiv \int_0^1 (1 - u/u_1)\, dy. \tag{17}$$

The value of x corresponding to a given λ can be calculated from the expression

$$\xi \equiv \frac{x}{R\mathfrak{R}} = -0.169 + 0.718u_1/u_m + 1.268\ln(u_m/u_1) - 0.550u_m/u_1 \tag{18}$$

by integrating equation 17:

$$u_m/u_1 = 1 - 2\lambda. \tag{19}$$

These equations are sufficient to determine the axial velocity, and Fig. 3 is a plot of u/u_m against r/R for various values of ξ. Note that the boundary layer retards more and more of the flow as ξ increases and since the total flux over the cross section is constant, the velocity in the core increases as a function of x and is always greater than the average velocity. The radius of the core region w is just $(1 - 5.74\lambda)^{\frac{1}{2}}$, as can be seen from equation 15, and this is plotted in Fig. 4 as a function of ξ. The displacement thickness of the boundary layer λ is also shown. It is readily seen that the boundary layer grows rather slowly, so that at $x/R = 1$ the core region still constitutes over half the cross-sectional area for $\mathfrak{R} \geq 250$ and over 10% for $\mathfrak{R} = 50$.

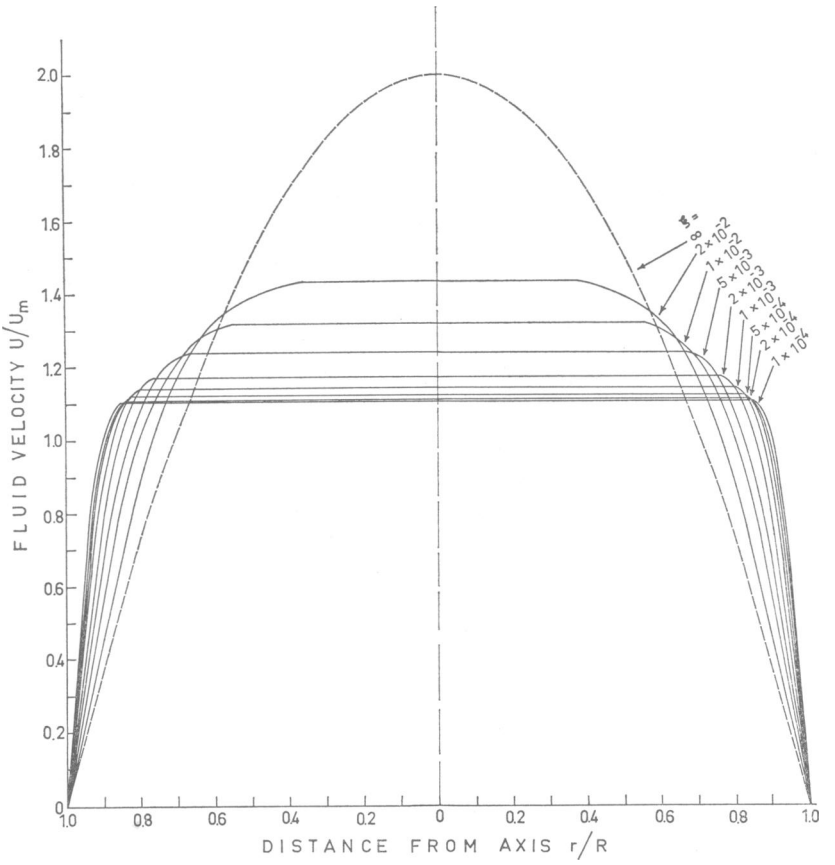

FIGURE 3 Fluid velocity u as a function of fractional distances r/R from orifice axis for various values of the parameter $\xi \equiv \mathfrak{R}^{-1} x/R$, where $\mathfrak{R}$ is tube Reynolds number and x/R is distance from mouth of orifice in units of orifice radius R. Velocity is expressed relative to mean linear velocity u_m. Dashed curve is velocity profile for complete parabolic flow.

The presence of the hydrodynamic field affects suspended particles in several ways. Superimposed on the orientation of nonspherical particles and the deformation of nonrigid spheres due to the potential gradient, as discussed in the previous section, there will now be orientation and deformation effects due to the velocity gradient of the fluid within the boundary layer. (The gradient in the axial direction within the core is very small and may be neglected.) More important, perhaps, this gradient will cause a migration of particles towards the core region.

Such a migration has been observed experimentally for both rigid (28–30) and nonrigid (31–33) spheres (28, 29, and 31) and spheroids (30, 32, and 33). (In the case of rigid spinning particles (28), the equilibrium position for fully developed parabolic flow far from the entrance (29) ($\xi > 0.26$) is not at the axis but somewhat removed from it. This tubular pinch effect is a function (30) of $\mathfrak{R}$ and a and is ex-

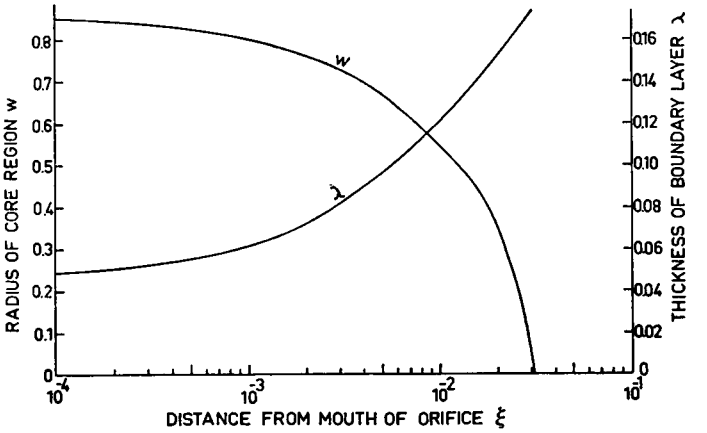

FIGURE 4 Radius of core region w and displacement thickness of boundary layer λ as functions of (dimensionless) distance from mouth of orifice ξ.

pected (34) to decrease for $\mathfrak{R} > 15$; there is some experimental evidence (29) to indicate that this is so.) Jeffery (35) considered the motion of rigid spheroids immersed in a viscous fluid and proposed that, of all motions satisfying his equations, the particles adopt that motion which corresponds to minimum energy dissipation. For motion in a capillary tube, this predicts that the particles will tend to concentrate within the core of the tube, and Starkey (36, 37) showed theoretically that this migration should increase with rate of shear and with particle size and distance from the axis. An approximate theory developed by Saffman (38) for rigid spheres that takes inertial effects into consideration but neglects the influence of the walls of the tube, gives the migration velocity u_r as

$$\frac{u_r}{u_m} = -3.44\mathfrak{R}\left(\frac{a}{R}\right)^4 \frac{r}{R}. \tag{20}$$

A more rigorous treatment (34) for the case

$$\frac{8}{3}\mathfrak{R}, 4\frac{r}{a}, 16\mathfrak{R}\frac{r}{a}, \frac{4}{9}\mathfrak{R}\frac{a}{R}, \frac{16}{9}\mathfrak{R}^2\frac{a}{r} \ll \left(\frac{R}{a}\right)^3 \tag{21}$$

gives

$$\frac{u_r}{u_m} = -\frac{324.8}{9\pi}\mathfrak{R}^{\frac{1}{2}}\left(\frac{a}{R}\right)^3\left(\frac{r}{R}\right)^{\frac{1}{2}}. \tag{22}$$

Theoretical and empirical expressions that include the effects of the walls are similar in form to equation 20 apart from the numerical coefficient, an additional factor to account for the tubular pinch effect, and the value of the exponent (30). The ex-

perimental evidence suggests that this last depends on the range of a/R: for $a/R \to 0$ its value (38) is 4, for $0.03 \leq a/R \leq 0.15$ it is (29) 2.84, for $0.25 \leq a/R \leq 0.30$ it is (30) 2.

If one substitutes typical values into the above expressions, one sees that all but one of the conditions of equation 21 hold, equation 22 giving a value of u_r/u_m of about 0.2. An examination of Fig. 3 (or Fig. 4) suggests that this value of u_r/u_m may be sufficient to exclude particles from the boundary layer. There are other considerations, both theoretical and experimental, which lend support to the idea that in many cases particles may concentrate exclusively within the core region. In the derivation of equation 22 a velocity gradient valid for complete parabolic flow was assumed, whereas in actual fact the boundary layer develops only rather slowly. The thinner the boundary layer, the higher the velocity gradient in that region, and thus a correction factor must be applied to equation 22. This correction factor is given by f, where

$$f^2 = \frac{0.571}{4\lambda(1 - 2\lambda)} \tag{23}$$

in the region where the first expression in equation 15 is applicable; in the region $0.63 \leq y/\lambda \leq 2.87$ it is given by f_1, where

$$f_1^2 = \frac{0.714}{4\lambda(1 - 2\lambda)} (1.025 - 0.357y/\lambda). \tag{24}$$

By introducing the factor f into equation 22, we find that $u_r \geq u_m$. Of course u_r gradually approaches zero as the particle leaves the boundary region, as is seen explicitly from equation 24.

The experimental consideration involves the observation (39) that as a particle enters a smaller tube from a larger one, it is displaced from the entering streamline towards the axis of the tube—the larger the particle and the nearer it is to the wall, the greater the displacement. This displacement, which may be due to interaction with the wall, can be quite substantial; displacements as large as five particle radii have been observed (39) from streamlines at $r/R = 0.92$ as the tube radius changed gradually by a factor of four over a distance equal to eight times the radius of the smaller tube.

The migration of nonrigid spheres due to their deformation in a velocity gradient has been studied theoretically and experimentally (31). The theoretical expression for the radial velocity was determined to be

$$\frac{u_r}{u_m} = -\frac{\pi\eta_2 u_m}{3\tau}\left(\frac{a}{R}\right)^3\left(\frac{r}{R}\right)g(p) \tag{25}$$

for $p \equiv \eta_1/\eta_2 \lesssim 20$, where η_1 is the viscosity of the particle and $g(p)$ is given by

$$g(p) = \frac{3(19p + 16)(40p^2 + 99p + 30)}{80(p + 1)(3p + 2)}, \tag{26}$$

but experimental results show that although equation 25 provides a good fit to the data, the dependence on p differs somewhat from equation 26. As the forces due to viscosity increase, the deformation becomes independent of u_m and τ, and theory (31, 40, and 41) predicts that

$$\frac{u_r}{u_m} = -\frac{\pi}{8}\left(\frac{a}{R}\right)^2 \frac{40p^2 + 99p + 30}{6p^2 + 13p + 6}. \tag{27}$$

In the event that the experimental conditions are such that the particle remains within the boundary layer, it is necessary to consider the effects of the velocity gradient on the orientation of spheroids and on the deformation of nonrigid particles. The first has been treated theoretically by Jeffery (35), who predicted that

$$\tan \psi - \tan \psi_0 = m \tan \frac{4mru_m}{(m^2 + 1)R^2} t, \tag{28}$$

giving a period of rotation T of

$$T = \frac{\pi(m^2 + 1)R}{2mu_m} \frac{R}{r}. \tag{29}$$

The experimental evidence (31) agrees well with these equations. If the electric and hydrodynamic forces are additive, then so are the rates of rotation due to each (15); that is, the combined rate of rotation $d\psi/dt$ is just $d\psi/dt$ obtained by differentiating equation 11 plus $d\psi/dt$ obtained by differentiating equation 28. The time required to rotate 180° is about 25 μsec under typical experimental conditions. As these equations have been developed for complete parabolic flow it is necessary, as discussed before, to correct for the increased velocity gradient in the boundary layer. Thus the argument in the right-hand side of equation 28 must be multiplied by (or T in equation 29 divided by) an appropriate correction factor which, in this case, is f^2 in the region $0 \leq y/\lambda \leq 0.63$ and f_1^2 in the region $0.63 \leq y/\lambda \leq 2.87$.

It remains to consider the effect of the velocity gradient on the deformation of nonrigid particles. An experimental investigation of this problem in complete parabolic flow has been carried out for small values of p and the results show (31) that at low gradients the sphere becomes prolate with an angle of inclination of 45° and a deformation given by

$$D = \frac{\eta_2 u_m}{4\tau} \frac{19p + 16}{p + 1} \frac{a}{R} \frac{r}{R}, \tag{30}$$

in agreement with theory (41). For larger gradients a better approximation (42) for ψ, confirmed experimentally for Couette flow (40), gives

$$\psi = \frac{\pi}{4} - D\left(1 + \frac{2}{5}p\right), \qquad \psi > 0. \tag{31}$$

Due to the increased gradient in the boundary layer, D must be multiplied by f^2 or f_1^2 as in the case of rotation, and substitution of typical values in equation 30 shows that the deformation can become considerable. As the velocity gradient and particle viscosity increase (but D remains small) the interfacial tension forces opposing deformation become negligible compared to those due to viscosity, the inclination approaches zero, and the deformation becomes independent of gradient, interfacial tension, and particle size (41)

$$D = \frac{5}{2}\frac{1}{2p + 3}. \tag{32}$$

This is the expression used to derive equation 27; it has been verified experimentally for Couette flow (40).

The combined deformation D_c due to both potential (D_p) and velocity (D_v) gradients is given by (18)

$$D_c^2 = D_p^2 - 2D_pD_v \cos 2\psi + D_v^2 \tag{33}$$

and the resultant inclination ψ_c is obtained from

$$\tan 2\psi_c = \frac{D_v \sin 2\psi}{D_v \cos 2\psi - D_p}. \tag{34}$$

We are now in a position to discuss the shape of the current pulse produced by a particle as it passes through the orifice in terms of the physical properties of the particle and the path it follows, and this is done below for the special case of rigid, nonconducting spheres and compared with actual measurements.

PULSE SHAPE

The potential within the orifice has been calculated under the assumption that the orifice is long enough for the electric field to attain a uniform value, and when this is so, the effect of the presence of a particle in the region of uniform field can be expressed as a change in the effective resistivity of the electrolyte. The passage of the particle through regions where the field is not uniform but depends on the x, r coordinates will give rise to relationships between the particle volume and the current change that are not as simple as that described by equation 5 but that depend on the electric field in those regions (Fig. 1).

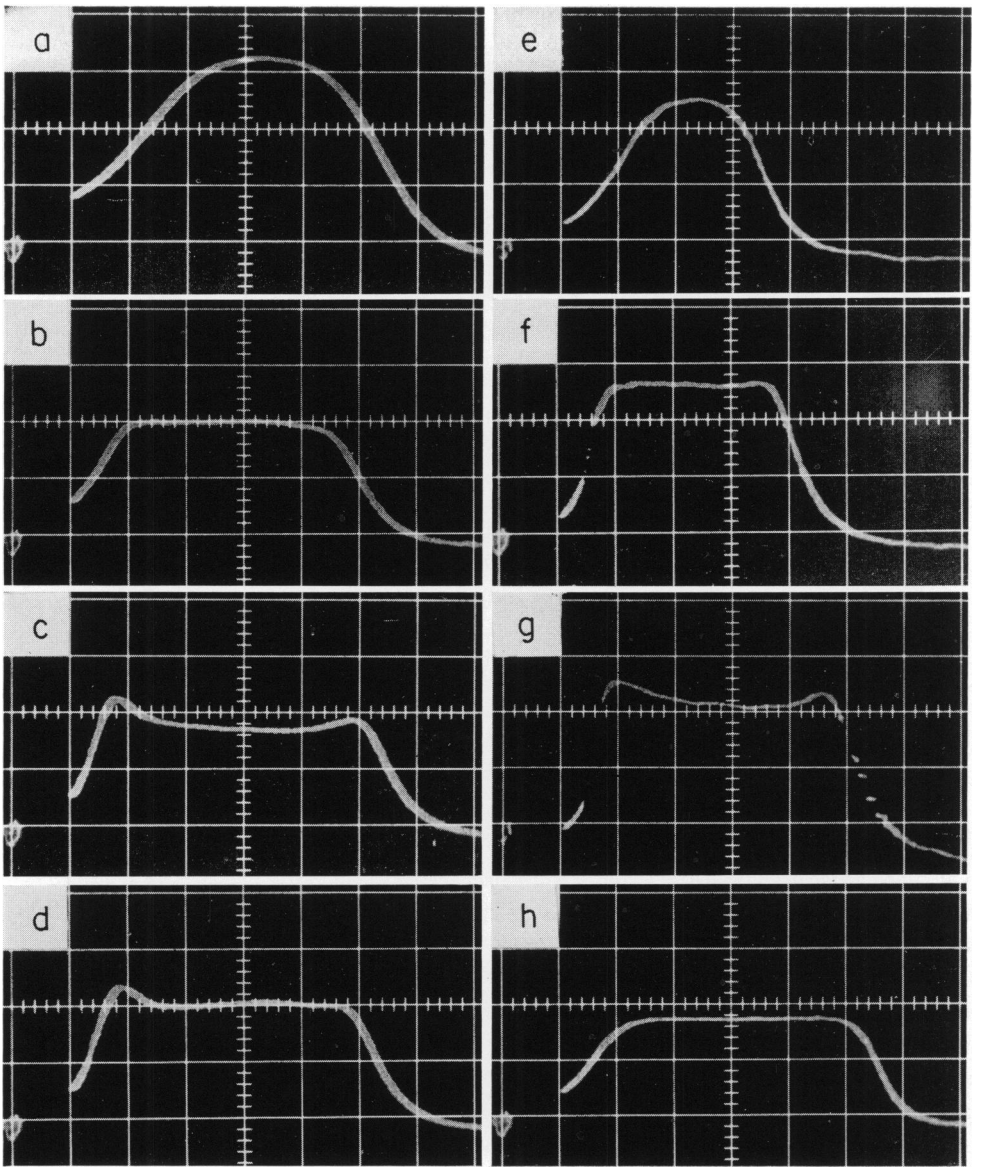

FIGURE 5 Oscillograms of pulse shapes with various particles and orifices. (*a–d*) Ragweed pollen, 200μ × 300μ orifice, 10 μsec/division sweep, 2.61 ma orifice current. (*e–g*) Polystyrene latex, 50μ × 80μ orifice, 5 μsec/division sweep, 6.25 ma orifice current. (*h*) Ragweed pollen, 50μ × 150μ orifice, 5 μsec/division sweep, 0.172 ma orifice current.

Fig. 5 illustrates the different types of current pulses produced by rigid, nonconducting spheres as they are pumped through cylindrical orifices of various sizes. Frames *a–c* are oscillograms of ragweed pollen in an orifice of 200 μ diameter and

300 μ length (nominal values); frames *e–g* show polystyrene latex particles in a 50 μ by 80 μ orifice (nominal). The three types of pulses shown for each particle, together with intermediate forms, comprise about 90% of all pulses monitored. (The remaining 10% is due to dirt particles and to coincidence pulses produced by the simultaneous presence within the orifice of more than one particle.)

The origin of these three types can be understood by referring to Fig. 1. Those particles that pass through the orifice within a distance of about 0.6 R from its axis will enter the region of uniform electric field only when they are quite near the center of the orifice; before entering and after leaving this region (the electric field, it will be recalled, is symmetrical about $L/2$, where L is the geometrical length of the orifice), they will experience a field that is lower. One would expect this to result in bell-shaped curves as in frames *a* and *e*. At distances between 0.6R and 0.8R the electric field is uniform along most of the length of the orifice, and we obtain plateau-like curves as in frames *b* and *f*. As the distance from the axis increases, the region of uniform electric field becomes narrower; particles outside this region now experience a field that is higher than the uniform field and so produce M-shaped pulses like those shown in frames *c* and *g*.

The general shape of each of the three types of pulses has been explained under the assumption that the path that a particle follows as it is pumped through the orifice is always parallel to the orifice axis. Such an assumption appears reasonable as long as the velocity of migration towards the orifice axis u_r is much smaller than the average velocity in the axial direction u_m. This will of course always be true while the particle remains in the core region, because there the velocity gradient is zero in the radial direction; it will also be true in the boundary layer provided the particle radius a is much smaller than the orifice radius R, as can be seen from equation 22. Substituting the experimental values into equation 22, one finds that for ragweed pollen ($a = 9.8\ \mu$) in the 200/300 orifice ($\mathfrak{R} \approx 400$) the migration velocity is about 25% of u_m while for the polystyrene latex particles ($a = 1.4\ \mu$) in the 50/80 orifice ($\mathfrak{R} \approx 100$), it is less than 2%. Thus a ragweed particle that enters the boundary layer as it passes through the orifice will migrate slowly towards the core region and so will leave the orifice nearer the axis than it entered it. Since any ragweed particle initially at $r \gtrsim 0.75\ R$ will have entered the boundary layer by the time it has passed halfway through the orifice (see Fig. 4), this suggests that one should expect such particles to produce pulses that are asymmetrical, their left halves corresponding to M-shaped pulses and their right halves to plateau-shaped pulses. Such a pulse is shown in frame *d*. Because there is almost no displacement in the case of the latex particles, no corresponding pulse shape is to be expected, and none was found.

The situation is quite different with ragweed in a 50/150 orifice ($\mathfrak{R} \approx 100$). Here $u_r > 5\ u_m$, and the ragweed is not able to leave the core region at all. Moreover because of the large ratio of length to radius in this orifice, the boundary layer develops rapidly (Fig. 3), confining the center of a ragweed particle to within 0.25 R

of the axis after it has passed through only 10% of the orifice length. Reference to Fig. 1 shows that in this range ($r/R \leq 0.25$, $x/R \geq 0.6$), the electric field is insensitive to r, resulting in a pulse shape independent of the distance from the axis at which the particle originally entered the orifice. Thus there will be only one type of pulse and, since the electric field is uniform throughout the inner 70% of the length of the orifice ($x/R \geq 0.9$), it will be plateau-shaped. (Actually, since the particle is nearly 40% of the orifice in diameter, it will experience a field that is some kind of average value taken over its surface; the resulting pulse will then be even less sensitive to radial variations in the field than Fig. 1 indicates.) Such a pulse, typical of all the pulses produced by ragweed particles in this orifice, is shown in frame *h*.

The above discussion has been restricted to the case of rigid, nonconducting spheres and has shown that there is good qualitative agreement between the pulse shapes obtained with such particles experimentally and those expected on the basis of the electrical and hydrodynamic considerations presented in the previous sections of this paper. The following paper (43) presents the results of a precise quantitative test of the theory for these particles and describes the experimental instrumentation used.

The authors wish to express their thanks to Professor N. Zeldes for several helpful discussions.

This investigation was supported in part by research grant CA-06582 from the National Cancer Institute, U. S. Public Health Service.

Received for publication 7 April 1969 and in revised form 17 July 1969.

REFERENCES

1. COULTER, W. H. 1953. U. S. Pat. No. 2,656,508. 1955. Brit. Pat. No. 722,418.
2. KUBITSCHEK, H. E. 1960. *Research (London).* **13**:128.
3. GREGG, E. C., and K. D. STEIDLEY. 1965. *Biophys. J.* **5**:393.
4. RAYLEIGH, LORD. 1945. The Theory of Sound. Macmillan & Co., New York. 2nd edition. **2**:175, 180.
5. SMYTHE, W. R. 1950. Static and Dynamic Electricity. McGraw-Hill Book Co., New York. 2nd edition. 232.
6. RAYLEIGH, LORD. 1945. The Theory of Sound. Macmillan & Co., New York. 2nd edition. **2**:487.
7. MAXWELL, J. C. 1954. A Treatise on Electricity and Magnetism. Dover Publications, Inc., New York. 3rd edition. **1**:437.
8. RAYLEIGH, LORD. 1892. *Phil. Mag.* **34**:481.
9. RUNGE, I. 1925. *Z. Tech. Physik.* **5**:61.
10. MEREDITH, R. E., and C. W. TOBIAS. 1960. *J. Appl. Phys.* **31**:1270.
11. FRICKE, H. 1924. *Phys. Rev.* **24**:575.
12. FRICKE, H. 1953. *J. Appl. Phys.* **24**:644.
13. FRICKE, H. 1953. *J. Phys. Chem.* **57**:934.
14. VELICK, S., and M. GORIN. 1940. *J. Gen. Physiol.* **23**:753.
15. DEMETRIADES, S. T. 1958. *J. Chem. Phys.* **29**:1054.
16. CHAFFEY, C. E., and S. G. MASON. 1964. *J. Colloid Sci.* **19**:525.
17. ALLAN, R. S., and S. G. MASON. 1962. *Proc. Roy. Soc. (London), Ser. A. Math. Phys. Sci.* **267**:62.
18. ALLAN, R. S., and S. G. MASON. 1962. *Proc. Roy. Soc. (London), Ser. A. Math. Phys. Sci.* **267**:45.
19. WEISS, L. 1967. The Cell Periphery, Metastasis, and Other Contact Phenomena. Holland, Uitgevers-Mij., Amsterdam. 248.

20. SCHWAN, H. P. 1957. *Advan. Biol. Med. Phys.* **5**:147.
21. HASTED, J. B., D. M. RITSON, and C. H. COLLIE. 1948. *J. Chem. Phys.* **16**:1.
22. TATSUMI, T. 1952. *J. Physiol. Soc. Japan.* **7**:489.
23. SMITH, A. M. O. 1960. *J. Fluid Mech.* **7**:565.
24. LANGHAAR, H. L. 1942. *J. Appl. Mech.* **9**:A55.
25. RESHOTKO, E. 1958. Progress Rep. No. 20-364. Jet Propulsion Laboratory, Pasadena, Calif.
26. PFENNINGER, W. 1951. Rep. No. AM-133, Northrop Aircraft Co., Beverly Hills, Calif.
27. NIKURADSE, J. (Unpublished). *See* Prandtl, L., and O. G. Tietjens. 1934. Applied Hydro- and Aeromechanics. McGraw-Hill Book Co., New York. 25.
28. OLIVER, D. R. 1962. *Nature.* **194**:1269.
29. SEGRÉ, G., and A. SILBERBERG. 1962. *J. Fluid Mech.* **14**:136.
30. KARNIS, A., H. L. GOLDSMITH, and S. G. MASON. 1966. *Can. J. Chem. Eng.* **44**:181.
31. GOLDSMITH, H. L., and S. G. MASON. 1962. *J. Colloid Sci.* **17**:448.
32. VEJLENS, G. 1938. *Acta Pathol. Microbiol. Scand., Suppl.* **33**:167.
33. KNISELY, M. H. 1960. *In* Flow Properties of Blood. A. L. Copley and G. Stainsby, editors. Pergamon Press, Oxford. 82.
34. SAFFMAN, P. G. 1965. *J. Fluid Mech.* **22**:385.
35. JEFFERY, G. B. 1922. *Proc. Roy. Soc. (London), Ser. A. Math. Phys. Sci.* **102**:161.
36. STARKEY, T. V. 1955. *Brit. J. Appl. Phys.* **6**:34.
37. STARKEY, T. V. 1956. *Brit. J. Appl. Phys.* **7**:52.
38. SAFFMAN, P. G. 1956. *J. Fluid Mech.* **1**:540.
39. KARNIS, A., and S. G. MASON. 1967. *J. Colloid Interface Sci.* **23**:120.
40. RUMSCHEIDT, F. D., and S. G. MASON. 1961. *J. Colloid Sci.* **16**:238.
41. TAYLOR, G. I. 1934. *Proc. Roy. Soc. (London), Ser. A. Math. Phys. Sci.* **146**:501.
42. CERF, R. 1951. *J. Chim. Phys.* **48**:59.
43. GROVER, N. B., J. NAAMAN, S. BEN-SASSON, F. DOLJANSKI, and E. NADAV. 1969. *Biophys. J.* **9**:1415.